Original Manuscript

Journal of Industrial Textiles

Volume 52: 1–14

DOI: 10.1177/15280837221121971
journals.sagepub.com/home/jit
SAGE

Styrene-ethylene-butadiene-styrene copolymer/carbon nanotubes composite fiber based strain sensor with wide sensing range and high linearity for human motion detection

Lele Li[1], Dongliang Li[1], Baojie Sun[1], Yanfen Zhou[1], Jianwei Ma[1], Shaojuan Chen[1], Liang Jiang[1] and Feng-Lei Zhou[1,2]

Abstract

Flexible strain sensors have attracted extensive attention due to their potential applications in wearable electronics and health monitoring. However, it is still a challenge to obtain flexible strain sensors with both high stretchability and wide linear strain sensing range. In this study, styrene-ethylene-butadiene-styrene copolymer/carbon nanotubes (SEBS/CNTs) composite fiber which showed both electrical conductivity and high stretchability was fabricated through a scalable wet spinning method. The effect of CNTs content on the strain sensing behavior of the SEBS/CNTs fiber based strain sensor was investigated. The results showed that when the CNTs content reached 7 wt%, the SEBS/CNTs composite fiber was capable of sensing strains as high as 500.20% and showed a wide linear strain sensing range of 0-500.2% with a gauge factor (GF) of 38.57. Combining high stretchability, high linearity and reliable stability, the SEBS/CNTs composite fiber based strain sensor had the ability to monitor the activities of different human body parts including hand, wrist, elbow, shoulder and knee.

[1]Qingdao University, Qingdao, China
[2]Centre for Medical Image Computing, University College London, London, UK

Corresponding authors:
Yanfen Zhou, College of Textiles and Clothing, Qingdao University, No.308 Ningxia Road, Qingdao 266071, China.
Email: yanfen.zhou@qdu.edu.cn
Liang Jiang, College of Textiles and Clothing, Qingdao University, No. 308 Ningxia Road, Qingdao 266071, China.
Email: liang.jiang@qdu.edu.cn

Keywords
Fiber, electrically conductive, strain sensing

Introduction

In recent years, flexible wearable electronic devices for detecting human physiological signals and body movement have made great progress.[1–3] Flexible strain sensors have been widely used for measuring and quantifying physiological and physical signals generated by human body.[4–8] Qualified flexible strain sensors should have excellent stretchability, high sensitivity and high durability.[5,9] Compared with metal based electronic devices which have excellent conductivity, electrically conductive polymer composites have the advantages of lightweight, softness and easily being processed into complex structures. Therefore, wearable strain sensors fabricated by combining the excellent properties of conductive fillers and polymer matrices have received widespread attention in recent years.[10] Various elastomers, such as polydimethylsiloxane (PDMS),[11] polyurethane (PU) and silicone rubber,[12,13] have been used as matrices for the fabrication of flexible strain sensors because of their high stretchability and good elastic recovery.[14] Carbon black (CB),[15] carbon nanotubes (CNTs),[11,16–19] silver nanowires (AgNWs),[17,20] and graphene have been used as conductive components due to their excellent electrical conductivity.[21–23] Among these conductive fillers, CNTs possessing both high electrical conductivity and excellent mechanical robustness are ideal for fabricating flexible strain sensors.[17,24–27]

Flexible strain sensors have been designed in the form of thin films, fabrics, and fibers.[10,28,29] In contrast to thin films and fabrics with two dimensional planar configurations, fiber based strain sensors have been developed extensively in recent years due to their special one dimensional structure and weaveability. For instance, Zhu et al.[30] prepared AgNWs embedded PU fibers through the capillary tube method, the composite fiber exhibited a response range of 43% and gauge factor (GF) of 87.6 up to 22% strain. Chen et al.[31] prepared graphene decorated PU fiber for strain sensor. Although the strain sensor showed a low detection limit (0.1% strain), the sensing range was very narrow (0–80%). Wang et al.[32] prepared poly(styrene-butadiene-styrene)/few layer graphene (SBS/FLG) composite fiber based strain sensor which showed a workable strain range up to 230%. Wang et al.[19] utilized the wet-spun method to prepare PU/MWCNTs fiber based strain sensor, which displayed a wide workable strain range of 320%, a relatively high GF of 22.2 within 160% strain and 97.1 for 160–320% strain. Cui et al.[33] fabricated stretchable strain sensors having a dentate groove structure based on CNTs decorated styrene-ethylene-butadiene-styrene copolymer (SEBS) filament. The maximum sensing strain was 240% and the linear sensing range was 0-90% with a GF of 0.12. The SEBS/CNT hybrid fibers based strain sensor reported by Zeng et al.[34] showed a wide strain sensing range of 0-471% and a GF of 368 at 471% strain.

Although a great deal of efforts have been made to improve the performances of composite fiber based strain sensors, it remains a big challenge to achieve a wide strain sensing range and high linearity simultaneously. In this work, a strain sensor based on

wet-spun SEBS/CNTs composite fiber was fabricated. SEBS was employed as the matrix because of its high stretchability, excellent elastic recovery, and good processability. CNTs was utilized as the conductive filler due to their excellent electrical properties, outstanding mechanical properties, and large aspect ratios. The SEBS/CNTs composite fiber based strain sensor showed a strain sensing range up to 0-500.2% and excellent linearity in this strain range. Furthermore, the sensing mechanism, the stability and its application in various human motion detection of the strain sensor were investigated.

Experimental

Materials

SEBS (Shore A hardness of 60) was provided by Kraton, USA. MWCNTs, with lengths of 10-20 μm, diameters of 4-6 nm and purity of 98% were purchased from Xianfeng nanomaterials technology Co., Ltd., China. Tetrahydrofuran (THF) and anhydrous ethanol were both provided by Sinopharm Chemical Reagent Co., Ltd., China.

Wet spinning of SEBS/CNTs Fiber

Firstly, the spinning solution consisting of SEBS, THF and CNTs was prepared by dispersing CNTs in THF under ultrasonic stirring for 2h, followed by adding SEBS to the above mixture. The whole mixture of CNTs, THF and SEBS were stirred magnetically at room temperature (about 10°C) for 18h, ultrasonically treated for 1h and then stirred magnetically for another 1h to ensure complete dissolving of SEBS and dispersion of CNTs. Then, the spinning solution was placed into a 10 mL syringe and extruded into the anhydrous ethanol coagulation bath with an extruding speed of 1.7 mL/h. Finally, the SEBS/CNTs fibers were dried in a vacuum oven at 30°C for 12h to ensure a complete removal of the solvent. The obtained composite fibers with different CNTs contents were denoted as SEBS/xCNTs, where x represents the mass fraction of CNTs in the composite fiber. For example, SEBS/3CNTs represents the composite fiber containing 3% CNTs.

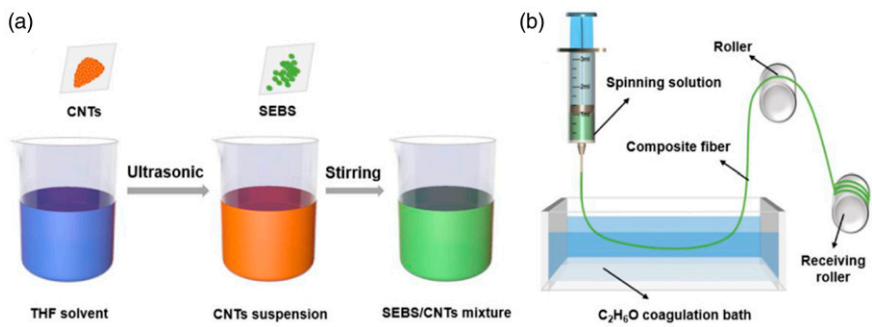

Figure 1. Schematic illustration for preparing SEBS/CNTs composite fiber.

The procedure for preparing SEBS/CNTs conductive composite fibers is shown in Figure 1.

Characterization

The surface and cross sectional morphology of the fibers were observed by using a Tescan Vega3 scanning electron microscope (SEM, Czech). A thin layer of gold was sputter coated on the samples before observation. The FTIR spectra were obtained by employing a Fourier transform infrared spectrometer (FTIR, Bruker TENSOR27, Germany). The Raman spectra was performed by using a Raman microscope (Thermo Scientific DXR2, America). The tensile properties of the fibers were tested by using an universal testing machine (Instron 5965, United States). The clamping distance of the sample was 20 mm and the tensile tests were performed at a speed of 100 mm·min^{-1}. The electrical and electromechanical properties of the fibers were measured by using a digital multimeter (B2901A Keysight, USA). A stepping motor was used to induce extension or cyclic extension-relaxation deformations. Samples were prepared by wrapping a copper tape at each end of the fiber and then connected with the digital multimeter to record the real time electrical resistance change.

Results and discussion

Morphology, mechanical property and electrical conductivity of SEBS/CNTs composite fiber

Figure 2 shows the longitudinal surface and cross-sectional morphology of the SEBS/CNTs fibers with CNTs contents of 3%, 5% and 7%. It can be seen that with the increase of CNTs content, the fiber surface became rougher. The SEBS/CNTs fiber had 'bean' shape cross section caused by the shrinkage of fiber during solidification. CNTs aggregates (as shown by the red dotted circles) could be observed on the cross section of the fiber, and the agglomeration phenomenon became more obvious as the content of CNTs increased.

The chemical composition of the composite fiber and possible interaction between SEBS and CNTs were studied by FTIR. It can be seen from Figure 3(a) that for pure SEBS fiber, there was a peak at 1457 cm^{-1}, which belongs to C-H in-plane bending vibration and C-C single bond skeleton vibration.[35] The peak at 2919 cm^{-1} belongs to C-H stretching vibration on saturated carbon;[36] For SEBS/CNTs fibers, a new absorption peak appeared near 3304 cm^{-1}, which was attributed to the stretching vibration of C-H on the unsaturated carbon double bond in CNTs,[37] indicating the existence of CNTs in SEBS matrix. In addition, the peaks originally located at 1457 cm^{-1} and 2919 cm^{-1} shifted to 1450 cm^{-1} and 2914 cm^{-1}, respectively. It can be inferred that there were some interactions between SEBS and CNTs.

Raman spectroscopy was employed to clarify the interactions between SEBS and CNTs. It can be seen from Figure 3(b) that the characteristic peaks of CNTs were 1339 cm^{-1} and 1585 cm^{-1}, which corresponded to typical D-band and G-band respectively, reflecting its graphite structure.[38,39] The crystal disorder in D-band is the main

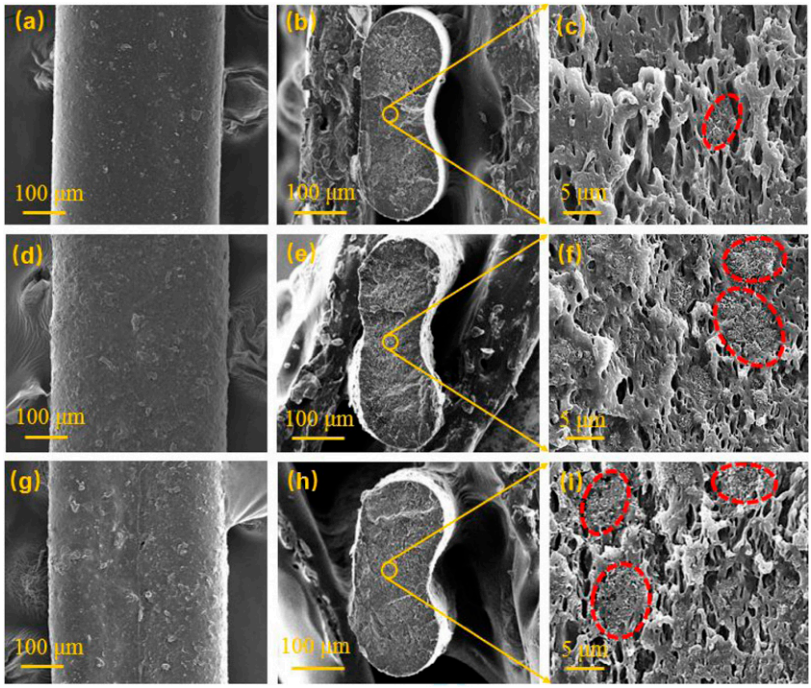

Figure 2. The surface and cross section morphology of SEBS/CNTs fibers with CNTs content of (a–c) 3%, (d–f) 5% and (g–i) 7%.

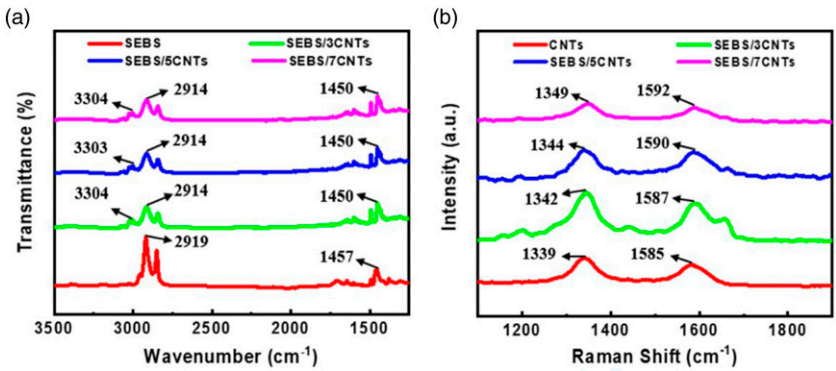

Figure 3. (a) FTIR spectra and (b) Raman spectra of SEBS and SEBS/xCNTs fibers.

Raman feature, and G-band represents the vibration of planar C-C bond.[40,41] Compared with CNTs, the peak centers of D-band of SEBS/3CNTs, SEBS/5CNTs and SEBS/7CNTs changed by 3 cm^{-1} (from 1339 cm^{-1} to 1342 cm^{-1}), 5 cm^{-1} (from 1339 cm^{-1} to

1344 cm^{-1}) and 10 cm^{-1} (from 1339 cm^{-1} to 1349 cm^{-1}) respectively. Those tiny changes indicate that there was a weak non-covalent π-π interface interaction between CNTs and SEBS matrix.[42,43]

Mechanical properties are very important for the practical application of fiber based strain sensors. Figure 4(a) and (b) shows respectively the typical stress-strain curves and the average values of tensile strength and elongation at break of SEBS/CNTs fibers with different CNTs contents. Compared with pure SEBS fiber, SEBS/CNTs composite fibers showed reduced mechanical properties. As the CNTs content increased from 3% to 7%, the tensile strength decreased from 37.66 ± 3.24 MPa to 27.46 ± 1.85 MPa and the elongation at break decreased from 1008.77 ± 83.62% to 772.87 ± 63.43%. This is because with the increase of CNTs content, more CNTs agglomerates were formed due to strong van der Waals force, which led to the decrease in mechanical properties.

The electrical conductivity of the composite fiber as a function of CNTs content is shown in Figure 4(d). It can be seen that the electrical conductivity of the fiber increased with increasing CNTs content. The relation between electrical conductivity and CNTs content was explored by employing the percolation theory (equation (1))[43]

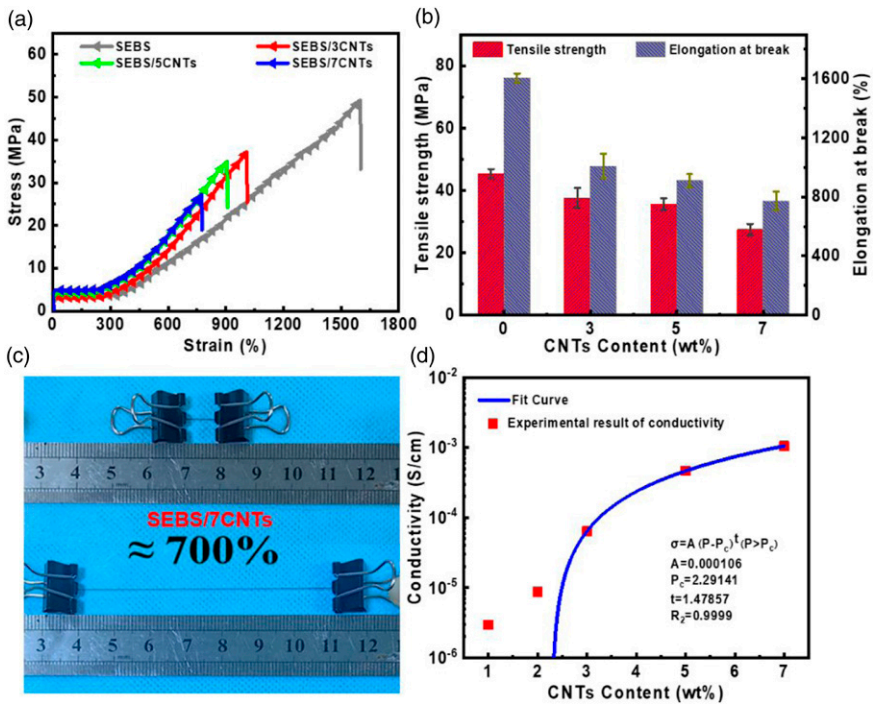

Figure 4. (a) Stress-strain curves, (b) tensile strength and elongation at break and (c) photographs of SEBS/CNTs fiber in original length and stretched state; (d) Electrical conductivity of SEBS/CNTs with different CNTs contents.

$$\sigma = A \cdot (P - P_c)^t \quad (\mathrm{P} > \mathrm{Pc}) \tag{1}$$

Where σ is the conductivity of the composite fiber, A is a scaling factor, P is the CNTs content, P_c is the percolation threshold, and t is the critical exponent depending on the geometry of the conducting network. The calculated percolation threshold was 2.29 wt%. Figure 4(c) shows the photographs of the SEBS/CNTs fiber in original length and in stretched state (with a strain of 700%) which intuitively showed the excellent stretchability of the fiber.

Electromechanical properties

The electromechanical properties of the SEBS/CNTs composite fiber based sensors were studied. Figure 5(a)-(c) shows the relative resistance change ($\Delta R/R_0$, $\Delta R = R\text{-}R_0$, R and R_0 represents the real-time and original resistance, respectively) as a function of strain for SEBS/CNTs composite fiber based sensors. It can be seen that for each fiber sensor,

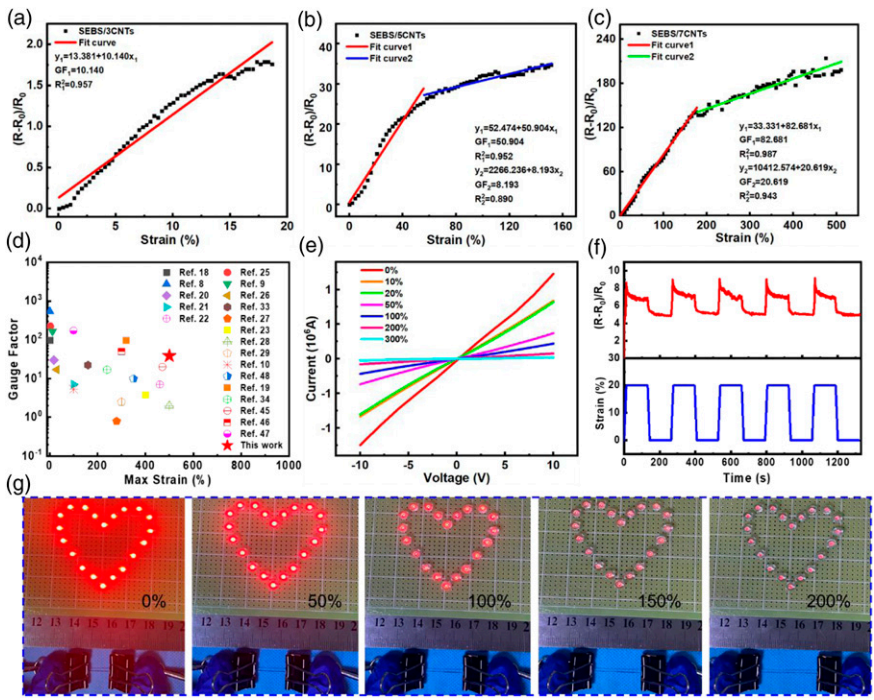

Figure 5. (a-c) The $(R\text{-}R_0)/R_0$-strain curves and GF of SEBS/CNTs composite fibers with different CNTs contents; (d) Comparison of the GF and the linear strain sensing range reported in the references and this work; (e) Current-voltage curves under different strain for SEBS/7CNTs fiber; (f) Relation between $(R\text{-}R_0)/R_0$ and time for SEBS/7CNTs fiber under 20% strain for five stretching-rest-releasing-rest cycles; (g) Changes in LED brightness when the SEBS/7CNTs fiber was stretched to strains of 0%, 50%, 100%, 150% and 200%.

$\Delta R/R_0$ increased with increasing strain, showing strain sensing characteristics. With the increase of CNTs content, the strain sensing range of the fiber sensor increased. The SEBS/7CNTs fiber sensor had a strain sensing range as wide as 0–500.2%. This is because the higher the content of CNTs, the more compact and complete the CNTs conductive networks inside the fiber, which needs larger deformation to be broken.

GF (GF = $\Delta R/(R_0 \cdot \varepsilon)$, ε is strain) was used to characterize the sensitivity of the composite fiber based sensors.[44–47] It can be seen from Figure 5(a) that SEBS/3CNTs fiber sensor had a GF of 10.14 in the strain range of 0–18.67%. The electrical response behaviour of SEBS/5CNTs fiber sensor could be divided into two linear regions: GF_1 of 50.90 at 0–55.67% strain and GF_2 of 8.19 at 55.67–151.67% strain (Figure 5(b)). The SEBS/7CNTs fiber sensor showed a high linearity (correlation coefficient of 0.992) in the sensing range of 0–500.2% with a GF of 38.57 (Figure 5(c)), which outperforms the recently reported stretchable strain sensors in respect of maximum sensing strain and linear strain sensing range (Figure 5(d)).

Figure 5(e) shows the current-voltage (I-V) curves of SEBS/7CNTs composite fiber at different strains. The linear I-V curves confirmed the excellent Ohmic characteristics of the composite fiber under stretching. It can also be seen from Figure 5(e) that under a specific applied voltage, the resistance of SEBS/7CNTs increased with increasing strain in the range of 0–300%, which further confirmed the strain response behavior.

To demonstrate the dynamic sensing behavior of SEBS/CNTs fiber based strain sensor, five cycles of stretching-rest-releasing-rest experiment was carried out, and the change of resistance with deformation was recorded and shown in Figure 5(f). It can be seen that $(R\text{-}R_0)/R_0$ increased with the increase of strain, when the strain was maintained at 20% for 120s, $(R\text{-}R_0)/R_0$ decreased gradually after reaching the maximum value and reached a stable value within 120s; When the strain was released, the $(R\text{-}R_0)/R_0$ decreased simultaneously. Notably, the $(R\text{-}R_0)/R_0$ at the end of the first cycle and the next four cycles was almost the same, revealing good repeatability.

To further demonstrate the tensile-resistance response behavior, a series circuit composed of a power source (B2901A Keysight), light emitting diode (LED) lights and the SEBS/7CNTs fiber was assembled. As can be seen from Figure 5(g), the brightness of the heart-shaped pattern composed of LED lights gradually dimmed as the tensile strain of the fiber increased up to 200%. This proves that the electrical resistance of SEBS/7CNTs fiber increased with increasing strain.

In practical application, dynamic reliability under different applied strains and different frequencies is essential for wearable strain sensors. Therefore, the dynamic strain sensing behavior was performed with a cyclic stretching-releasing under different strains (10%, 20%, 50%, 100%, 200%, 300%), and at different strain rates (5, 10, 20, 50, 100, 200, 300 and 400 mm/min). As can be seen from Figure 6, the SEBS/7CNTs fiber had a stable response under different strains ranges and different tensile rates.

To evaluate the durability and reproducibility of the SEBS/7CNTs based strain sensor, 7500 stretching-releasing cycles were tested at a constant strain range of 0–10% with a tensile speed of 20 mm/min, the change of $(R\text{-}R_0)/R_0$ with cycles is shown in Figure 7(a). It can be seen that the $(R\text{-}R_0)/R_0$ increased slowly as the number of stretching-releasing cycles increased, but the shape of the signal remained similar.

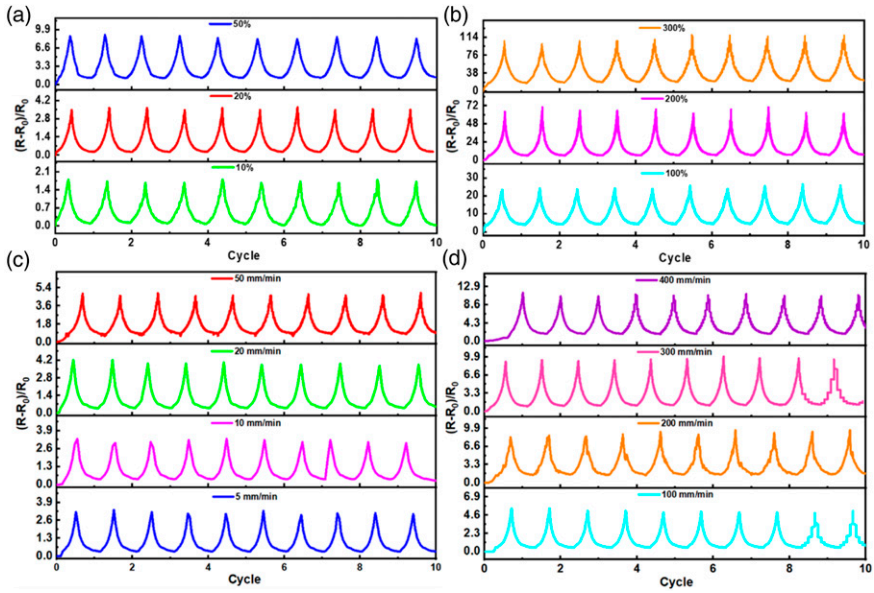

Figure 6. (a-b) Dynamic response behaviors of SEBS/7CNTs sensor at different strains under a fixed tensile speed of 10 mm/min; (c-d) Dynamic response behaviors of SEBS/7CNTs sensor under different tensile speed at a fixed strain range of 0–20%.

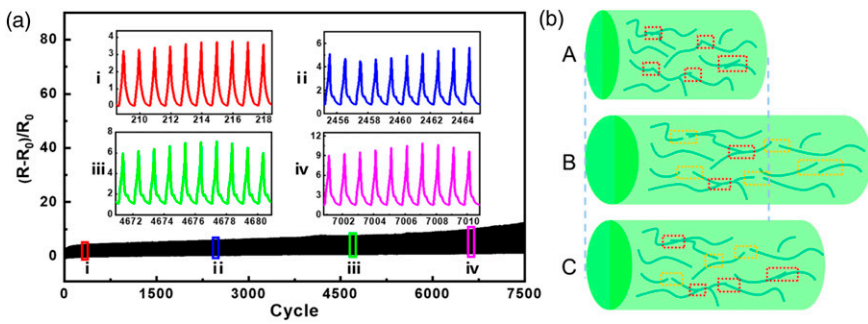

Figure 7. (a) Relative change of electrical resistance during 7500 stretching-releasing cycles at 20% strain and 20 mm/min strain rate, the illustrations in (a) are enlarged views of the stretching-releasing cycles at different stages; (b) Schematic illustration for the evolution of the CNTs conductive network during the stretching-releasing process. A. The initial state; B. the stretching state; C. the releasing state.

The evolution of CNTs conductive network during the stretching-releasing process was schematically presented to explain the mechanism of electrical resistance change (Figure 7(b)). Before extension, the CNTs conductive network in the composite fiber was compact (Figure 7(b) (A)), and the electrical resistance was the lowest. During the cyclic

stretching-releasing test, the destruction and reconstruction of the CNTs conductive networks in the SEBS/CNTs fiber changed periodically with the applied strain due to the periodical change of the distance between adjacent CNTs. When the fiber was stretched, the distance between two adjacent carbon nanotubes increased with increasing strain, the CNTs-CNTs coincidence point in the dense CNTs network was gradually destroyed when the distance between CNTs was greater than the critical distance, meanwhile, new CNTs-CNTs contacting points formed (Figure 7(b) (B)). As the destruction of the CNTs network predominant in the stretching process, $(R\text{-}R_0)/R_0$ increased with increasing strain. When the fiber was released, the distance between adjacent CNTs decreased, the CNTs conductive networks reconstructed when the distance between CNTs was less than the critical distance (Figure 7(b) (C)), the $(R\text{-}R_0)/R_0$ of SEBS/7CNTs strain sensor decreased with releasing strain. Due to the continuous destruction and reconstruction of CNTs conductive networks in the stretching-releasing process, partial conductive pathways might be destroyed and hence the $(R\text{-}R_0)/R_0$ showed a slight upward trend as shown in Figure 7(a).

Application for human motion detection

The excellent electromechanical properties of the SEBS/7CNTs strain sensors endowed their use in wearable devices for human motion detection. A consent form was read and signed by the participants before the test. Figure 8(a) shows the real-time monitoring of human finger movement and the bending of interphalangeal joints at different angles of 30°, 60°, 90° and 120°, respectively. It can be seen that the value of $(R\text{-}R_0)/R_0$ increased with the bending of interphalangeal joint and decreased with the straightening of joint. In addition, the maximum value of $(R\text{-}R_0)/R_0$ increased with the increase of angle, indicating

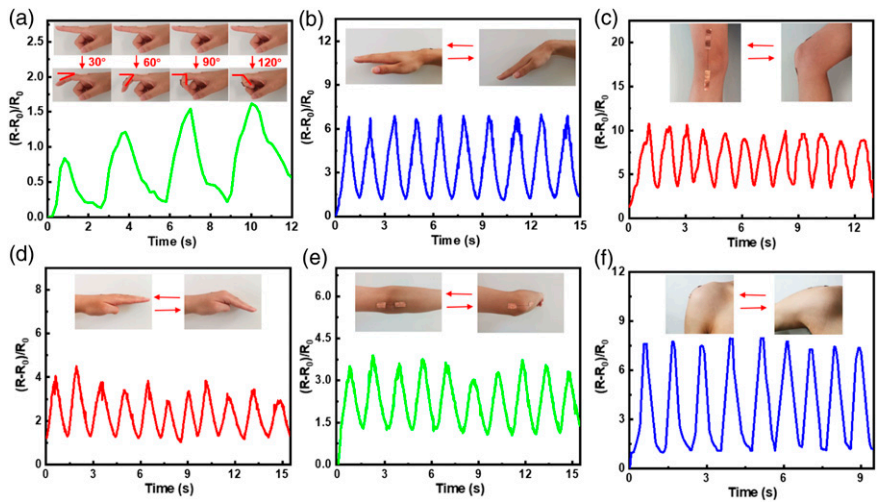

Figure 8. Human motion monitoring. (a) Finger bending test at different angles, (b) wrist bending, (c) knee bending, (d) back of hand bending, (e) arm bending and (f) shoulder movement.

that different degrees of bending deformation can be distinguished in time. As shown in Figure 8(b)-(d), the real-time monitoring of human wrist, knee and back of hand bending for 60° and extension was recorded respectively. Figure 8(e) and (f) shows the motion monitoring of arm and shoulder bending for 90°. It can be seen that SEBS/7CNTs strain sensor could successfully capture the bending signals of different parts, $(R\text{-}R_0)/R_0$ rose with the increase of bending and returned to the initial value after the bending was released. These results showed that the sensor based on SEBS/7CNTs fiber had the ability to detect small and large-scale movement of different human body parts.

Conclusion

Highly stretchable SEBS/CNTs composite fibers were fabricated through wet spinning and their application in strain sensors was evaluated. The results showed the CNTs content had important influence on the strain sensing performances of the composite fiber. The SEBS/7CNTs fiber based strain sensor showed the widest strain sensing range of 0-500.2% with a high linearity in the whole sensing range. The composite fiber with 5% CNTs also exhibited the ability to sense strains of above 150%. Furthermore, the SEBS/CNTs fiber based strain sensor showed reliable stability when subjected to 7500 cycles of stretching-releasing deformations. Finally, it was demonstrated that the SEBS/CNTs composite fiber based sensor had the ability to detect the activities of different human body parts including hand, wrist, elbow, shoulder and knee.

Acknowledgements

The authors thank the financial support from the National Natural Science Foundation of China (Grant no. 52003130), the Shandong Provincial Natural Science Foundation (Grant no. ZR2020QE087) and the Shandong "Taishan Youth Scholar Program" (Grant no. tsqn201909100).

Declaration of conflicting interests

The author(s) declared no potential conflicts of interest with respect to the research, authorship, and/or publication of this article.

Funding

The author(s) disclosed receipt of the following financial support for the research, authorship, and/or publication of this article: National Natural Science Foundation of China (Grant no. 52003130), the Shandong Provincial Natural Science Foundation (Grant no. ZR2020QE087) and the Shandong "Taishan Youth Scholar Program" (Grant no. tsqn201909100).

ORCID iDs

Yanfen Zhou https://orcid.org/0000-0002-3020-6101
Liang Jiang https://orcid.org/0000-0002-7792-6069
Feng-Lei Zhou https://orcid.org/0000-0002-8348-4658

References

1. Soh PJ, Vandenbosch G, Mercuri M, et al. Wearable Wireless health monitoring: current developments, challenges, and future trends. *IEEE Microwave Mag* 2015; 16(4): 55–70.
2. Pang Y, Yang Z, Yang Y, et al. Wearable electronics based on 2D materials for human physiological information detection. *Small* 2020; 16(15): 1901124.
3. Liu M, Pu X, Jiang C, et al. Large-area all-textile pressure sensors for monitoring human motion and physiological signals. *Adv Mater* 2017; 29(41): 1703700.
4. Liu Y, Wang H, Zhao W, et al. Flexible, stretchable sensors for wearable health monitoring: sensing mechanisms, materials, fabrication strategies and features. *Sensors* 2018; 18(2): 645.
5. Trung TQ and Lee N. Flexible and stretchable physical sensor integrated platforms for wearable human-activity monitoringand personal healthcare. *Adv Mater* 2016; 28(22): 4338–4372.
6. Guo X, Huang Y, Zhao Y, et al. Highly stretchable strain sensor based on SWCNTs/CB synergistic conductive network for wearable human-activity monitoring and recognition. *Smart Mater Struct* 2017; 26(9): 095017.
7. Wang Y, Zhu M, Wei X, et al. A dual-mode electronic skin textile for pressure and temperature sensing. *Chem Eng J* 2021; 425(6212): 130599.
8. Liao X, Liao Q, Yan X, et al. Flexible and highly sensitive strain sensors fabricated by pencil drawn for wearable monitor. *Adv Funct Mater* 2015; 25(16): 2395–2401.
9. Shi G, Zhao Z, Pai J, et al. Highly sensitive, wearable, durable strain sensors and stretchable conductors using graphene/silicon rubber composites. *Adv Funct Mater* 2016; 26(42): 7614–7625.
10. Chen S, Lou Z, Chen D, et al. Polymer-enhanced highly stretchable conductive fiber strain sensor used for electronic data gloves. *Adv Mater Tech* 2016; 1(7): 1600136.
11. Li T, Li J, Zhong A, et al. A flexible strain sensor based on CNTs/PDMS microspheres for human motion detection. *Sensors Actuators A: Phys* 2020; 306: 111959.
12. Nag A, Alahi M, Mukhopadhyay S, et al. Multi-walled carbon nanotubes-based sensors for strain sensing applications. *Sensors* 2021; 21(4): 1261.
13. Huang L, Wang H, Wu P, et al. Wearable flexible strain sensor based on three-dimensional wavy laser-induced graphene and silicone rubber. *Sensors* 2020; 20(15): 126959.
14. Cai S, Xu C, Jiang D, et al. Air-permeable electrode for highly sensitive and noninvasive glucose monitoring enabled by graphene fiber fabrics. *Nano Energy* 2022; 93: 106904.
15. Yan T, Wang Z and Pan Z. Flexible strain sensors fabricated using carbon-based nanomaterials: a review. *Curr Opin Solid State Mater Sci* 2018; 22(6): 213–228.
16. Zhao S, Yan Y, Gao A, et al. Flexible polydimethylsilane nanocomposites enhanced with a three-dimensional graphene/carbon nanotube bicontinuous framework for high-performance electromagnetic interference shielding. *ACS Appl Mater Inter* 2018; 10(31): 26723–26732.
17. Li L, Du Z, Sun B, et al. Fabrication of electrically conductive poly(styrene-b-ethylene-ran-butylene-b-styrene)/multi-walled carbon nanotubes composite fiber and its application in ultra-stretchable strain sensor. *Eur Polym J* 2022; 169: 111121.
18. Zhou B, Li C, Zhou Y, et al. A flexible dual-mode pressure sensor with ultra-high sensitivity based on BTO@MWCNTs core-shell nanofibers. *Composites Sci Technol* 2022; 224: 109478.

19. Wang X, Sun H, Yue X, et al. A highly stretchable carbon nanotubes/thermoplastic polyurethane fiber-shaped strain sensor with porous structure for human motion monitoring. *Composites Sci Technol* 2018; 168(10): 126–132.
20. Park M, Im J, Shin M, et al. Highly stretchable electric circuits from a composite material of silver nanoparticles and elastomeric fibres. *Nat Nanotechnol* 2012; 7(12): 803–809.
21. Yan C, Wang J, Kang W, et al. Highly stretchable piezoresistive graphene-nanocellulose nanopaper for strain sensors. *Adv Mater* 2014; 26(13): 2022–2027.
22. Lee P, Ham J, Lee J, et al. Highly stretchable or transparent conductor fabrication by a hierarchical multiscale hybrid nanocomposite. *Adv Funct Mater* 2014; 24(36): 5671–5678.
23. Muth J, Vogt D, Truby R, et al. Embedded 3D printing of strain sensors within highly stretchable elastomers. *Adv Mater* 2014; 26(36): 6307–6312.
24. Wei X, Zhu M, Li J, et al. Wearable biosensor for sensitive detection of uric acid in artificial sweat enabled by a fiber structured sensing interface. *Nano Energy* 2021; 85: 106031.
25. Liu X, Tang C, Du X, et al. A highly sensitive graphene woven fabric strain sensor for wearable wireless musical instruments. *Mater Horizons* 2017; 4(3): 477–486.
26. Wang M, Zhang K, Dai X, et al. Enhanced electrical conductivity and piezoresistive sensing in multi-wall carbon nanotubes/polydimethylsiloxane nanocomposites via the construction of a self-segregated structure. *Nanoscale* 2017; 9(31): 11017–11026.
27. Yamada T, Hayamizu Y, Yamamoto Y, et al. A stretchable carbon nanotube strain sensor for human-motion detection. *Nat Nanotechnol* 2011; 6(5): 296–301.
28. Amjadi M, Yoon Y and Park I. Ultra-stretchable and skin-mountable strain sensors using carbon nanotubes-Ecoflex nanocomposites. *Nanotechnology* 2015; 26(37): 375501.
29. Travas Sejdic J, Giffney T, Kurian AS, et al. Highly stretchable printed strain sensors using multi-walled carbon nanotube/silicone rubber composites. *Sensors Actuators A: Phys* 2017; 259: 44–49.
30. Zhu G, Ren P, Guo H, et al. Highly sensitive and stretchable polyurethane fiber strain sensors with embedded silver nanowires. *ACS Appl Mater Inter* 2019; 11(26): 23649–23658.
31. Chen Y, Zhang Y, Song F, et al. Graphene decorated fiber for wearable strain sensor with high sensitivity at tiny strain. *Adv Mater Tech* 2021; 6(12): 2100421.
32. Wang X, Meng S, Tebyetekerwa M, et al. Highly sensitive and stretchable piezoresistive strain sensor based on conductive poly(styrene-butadiene-styrene)/few layer graphene composite fiber. *Composites Part A: Appl Sci Manuf* 2018; 105: 291–299.
33. Cui X, Jiang Y, Xu Z, et al. Stretchable strain sensors with dentate groove structure for enhanced sensing recoverability. *Composites Part B: Eng* 2021; 211(9): 108641.
34. Zeng J, Ma W, Wang Q, et al. Strong, high stretchable and ultrasensitive SEBS/CNTs hybrid fiber for high-performance strain sensor. *Composites Commun* 2021; 25: 100735.
35. Sen P, Suresh K, Vinoth Kumar R, et al. A simple solvent blending coupled sonication technique for synthesis of polystyrene (PS)/multi-walled carbon nanotube (MWCNT) nanocomposites: effect of modified MWCNT content. *J Sci Adv Mater Devices* 2016; 1(3): 311–323.
36. Singla T, Pal Singh A, Kumar S, et al. Characterization of MWCNTs-polystyrene nanocomposite based strain sensor. *Proc Inst Mech Eng Part E: J Process Mech Eng* 2020; 235(2): 463–469.

37. Viswanathan K, Ravi T, Thirusakthimurugan P, et al. Carbon nanotube embedded smart polymer composite for strain and piezo-resistive data transducer application. *Mater Today Proc* 2018; 5(9): 17247–17252.
38. Wang L, Chen Y, Lin L, et al. Highly stretchable, anti-corrosive and wearable strain sensors based on the PDMS/CNTs decorated elastomer nanofiber composite. *Chem Eng J* 2019; 362: 89–98.
39. Zhang X, Qasim K and Hu S. Enhanced piezoresistance repeatability of carbon nanotube/silicane composites achieved using radiation-induced graft polymerization. *J Polym Res* 2014; 21(6): 479.
40. Ramalingame R, Bautista-Quijano J, Alves D, et al. Temperature self-compensated strain sensors based on MWCNT-graphene hybrid nanocomposite. *J Composites Sci* 2019; 3(4): 96.
41. Ku-Herrera J, Avilés F, Nistal A, et al. Interactions between the glass fiber coating and oxidized carbon nanotubes. *Appl Surf Sci* 2015; 330: 383–392.
42. Kuester S, Barra G and Demarquette N. Morphology, mechanical properties and electromagnetic shielding effectiveness of poly(styrene-b-ethylene-ran-butylene-b-styrene)/carbon nanotube nanocomposites: effects of maleic anhydride, carbon nanotube loading and processing method. *Polym Int* 2018; 67(9): 1229–1240.
43. Yu S, Wang X, Xiang H, et al. Superior piezoresistive strain sensing behaviors of carbon nanotubes in one-dimensional polymer fiber structure. *Carbon* 2018; 140: 1–9.
44. Zhou B, Liu Z, Li C, et al. A highly stretchable and sensitive strain sensor based on dopamine modified electrospun SEBS fibers and MWCNTs with carboxylation. *Adv Electron Mater* 2021; 7(8): 2100233.
45. Wang Y, Li W, Li C, et al. Fabrication of ultra-high working range strain sensor using carboxyl CNTs coated electrospun TPU assisted with dopamine. *Appl Surf Sci* 2021; 566: 150705.
46. Wang C, Xia K, Jian M, et al. Carbonized silk georgette as an ultrasensitive wearable strain sensor for full-range human activity monitoring. *J Mater Chem C* 2017; 5(30): 7604–7611.
47. Gong S, Lai D, Su B, et al. Highly stretchy black gold E-Skin nanopatches as highly sensitive wearable biomedical sensors. *Adv Electron Mater* 2015; 1(4): 1400063.